NASA CONTRACTOR REPORT

NASA CR-131

NASA CR-131

N65-11044
52
1
CR-131

COMPRESSIBILITY EFFECTS ON FLUID ENTRAINMENT BY TURBULENT MIXING LAYERS

by Jacques A. F. Hill and James E. Nicholson

Prepared under Contract No. NASw-601 *by*
MITHRAS, INC.
Cambridge, Mass.
for

NATIONAL AERONAUTICS AND SPACE ADMINISTRATION • WASHINGTON, D. C. • NOVEMBER 1964

COMPRESSIBILITY EFFECTS ON FLUID ENTRAINMENT BY TURBULENT MIXING LAYERS

By Jacques A. F. Hill and James E. Nicholson

Distribution of this report is provided in the interest of information exchange. Responsibility for the contents resides in the author or organization that prepared it.

Prepared under Contract No. NASw-601 by
MITHRAS, INC.
Cambridge, Massachusetts

for

NATIONAL AERONAUTICS AND SPACE ADMINISTRATION

For sale by the Office of Technical Services, Department of Commerce,
Washington, D.C. 20230 -- Price $1.50

TABLE OF CONTENTS

LIST OF ILLUSTRATIONS

COMPRESSIBILITY EFFECTS ON FLUID ENTRAINMENT BY TURBULENT MIXING LAYERS

SUMMARY

11044

Fluid entrainment by supersonic turbulent mixing layers has been measured on a wind-tunnel model over a wide range of Mach numbers and ratios of the densities of the moving and stationary fluids.

The wind-tunnel model consisted of a forward-facing spike on a flat-faced cylinder. In the supersonic airstream this geometry generated a conical region of separated flow bounded by a constant-pressure mixing layer. By detecting whether or not there was any recirculation at the reattachment line, it was possible to supply fluid to the separated region at the same rate at which it was entrained by the mixing layer. The entrainment coefficient of the mixing layer could thus be calculated by metering the fluid supplied.

Supplying both air and helium to the mixing layer, it was found empirically that all the data could be correlated by the formula

$$c_q = 0.049 \left(\frac{\rho_i}{\rho_e}\right)^{0.4} \left(1 + \frac{\gamma - 1}{2} M_e^2\right)^{-0.67}$$

within ± 10 percent. (Symbols are defined in Appendix A.)

Numerical calculations of mixing-layer profiles have been made in order to allow a comparison of these measurements with the values of the spreading parameter, σ, quoted in the literature. Three different laws were considered for the effect of compressibility on the formula for the eddy viscosity. One was rejected for yielding profile shapes inconsistent with experiment and the other two gave nearly identical results.

For the case of isoenergetic entrainment of air by air, the only case for which other data are available, the measurements and calculations reported have predicted that σ increases with Mach number according to the formula

$$\sigma \propto \left(1 + \frac{\gamma - 1}{2} M^2\right)^{0.29}$$

This result falls somewhat below most of the other data available.

Author

INTRODUCTION

When one stream of fluid flows over another moving at a different speed, a mixing layer forms at the interface in much the same way as a boundary layer forms in the flow over a solid surface. Like the flow in a boundary layer, the flow in a mixing layer is a shear flow and it may be either laminar or turbulent, according as the Reynolds number is low or high.

The investigation reported here is concerned with a special class of turbulent mixing layers in which one of the fluid streams is at rest. The classic example of this kind of flow is often called the half-jet and is formed from the separating boundary layer of the flow issuing from a nozzle into a quiescent gas, as illustrated in Fig. 1. The cases considered here include some in which the flowing and quiescent gases are different.

The low speed half-jet flow has been the subject of several analytical investigations, of which the first was conducted by Tollmien (Ref. 1) in 1926. The basic features of this flow are

1) the flow is self-similar; the velocity profile shape is invariant along the layer
2) the rate of increase of the width of the layer is linear
3) fluid is entrained from the quiescent side of the layer at a rate which is invariant along the layer

The analytical treatment requires some empirical assumption about the relation of the turbulent shear stress to the local velocity gradient. Various assumptions have been used, all which lead to approximately the same velocity profile shape. Any expression for the shear stress contains a constant which the theory leaves undetermined so that its value must be determined from experiment. This constant appears both in the formula for the rate of growth of the layer and in that for the rate of fluid entrainment from the quiescent side. It also appears in the scaling law for the self-similar profile and is most often determined in terms of the scale factor which gives the best fit of the measurements to this profile.

Analyses of the mixing layer in compressible flow require a further assumption about the influence of the density variation across the layer on the shear stress. At least three different formulas have been suggested and used for calculations. The empirical constant is not necessarily invariant and must be determined by a series of experimental measurements

covering the full range of interest of the basic flow parameters such as Mach number, temperature ratio across the layer, and so on.

On the experimental side, there have been about half a dozen investigations of the incompressible half-jet since 1926. The values of the basic constant determined from these measurements agree within about ± 10 percent.

A summary of the available data for compressible flows has been published by Maydew and Reed (Ref. 2). The range of Mach numbers represented extends almost up to M ≈ 3. There are two significant restrictions on the scope of the data, however,

a) both the flowing and quiescent fluids are air

b) the flows are all isoenergetic; the total enthalpy of the flowing stream is equal to that of the quiescent air.

WIND TUNNEL MEASUREMENTS

Basic Technique

This investigation of turbulent mixing layers was based on measurements of the rate of fluid entrainment from the "dead-water" region adjoining the inner edge. This was in contrast to the commonly-used method of measuring velocity profiles and fitting them to a theoretical curve. Either kind of measurement can be analyzed equally well to supply the undetermined empirical constant in a theoretical treatment of turbulent mixing layers.

Figure 2 is a schematic illustration of the flow geometry used. A spike was used to create a conical region of separated flow ahead of a flat-faced cylindrical model mounted in a wind tunnel. The mixing layer constituted the conical surface separating the "dead-water" region on the inside from the supersonic flow on the outside. Gas was supplied to the separated region from a metered supply outside the tunnel through small perforations in the hollow spike.

The technique for measuring the rate of fluid entrainment was similar to that used by Ricou and Spalding (Ref. 3) in their investigation of fluid entrainment by fully developed turbulent jets. The essence of this technique is the detection of the condition that the gas supplied to the separated region exactly matches the amount entrained by the mixing layer. As described by Chapman (Ref. 4) and others, the flow will adjust itself to the rate of fluid injection. If too little is injected, the mixing layer will reattach to the body and some of the fluid in the layer will recirculate back into the separated region. If too much is injected, the mixing layer will be blown entirely off the body and some of the injected gas will escape from the separated region

by flowing back along the body under the mixing layer. Thus by detecting both recirculation of fluid into and escape of fluid from the separated region, it is possible to adjust the gas supply so that neither occurs and the entrainment by the mixing layer is matched. A pair of Stanton tubes on the face of the model, installed as described below, was used for this purpose.

In addition to metering the total flow entrained by the mixing layer, the wind-tunnel model was designed to measure the distribution of entrainment along the layer. For this purpose three discs were mounted on the spike, as shown in Fig. 2, dividing the separated region into four compartments. By constructing the hollow spike out of four concentric tubes, each compartment was provided with an individual gas supply.

To measure the distribution of entrainment along the layer, each gas supply was individually matched to the rate of entrainment from its own compartment. A pressure measurement in each compartment was used to set up this condition. A mismatch in any one compartment required in-flow or out-flow across one of the discs and hence a pressure differential across this disc. Adjustment of the flow rates, until all the pressures were balanced, assured the desired matching of injection to entrainment in each compartment.

Model

The basic wind tunnel model is shown in Fig. 3. The model is comprised of a spike of approximately 7.4 inches mounted on a 4.22 inch diameter body forming the altitude and base of a 16° cone. The spike length was chosen so that the conical displacement surface formed by the mixing layer would be approximately 20°. The region between the 20° conical tip and the model was divided into four compartments by three thin circular discs.

In order to detect the differential pressures, a series of pressure probes were installed along a 10° conical ray from the model tip. In a similar manner, one thermocouple was installed in each of the forward three compartments. The thermocouples served as an additional indication that free stream air was not recirculating into the dead-air region formed by isolating discs. This measurement was of value when the tunnel recovery temperature differed greatly from the injected gas temperature.

A pair of Stanton-tubes was mounted on the model face, one pointing inward and one outward, along a radial ray. When gas recirculated into the last compartment, the outward facing tube detected a greater pressure than the inward facing tube. The converse was true when too much gas was supplied to the mixing layer. When there was no pressure difference across the three isolating discs and the pair of Stanton tubes, the entrainment requirement of the mixing layer was satisfied exactly.

The basic three isolating discs were located along a 13° conical ray angle. Two sets of rings were used to increase the disc angle to 14° or 15°. During the wind tunnel program all three disc sets were used to determine

the effect of disc size on entrainment rate. In general, the 15° disc set had a large effect on the entrainment coefficient whereas the entrainment coefficient was invariant when the small and medium sets were used. The effect of disc size was most apparent at the low Mach numbers with the helium injectant. The helium-air mixing layer spreads at such a large angle that the isolating discs actually protruded into the free layer and interfered with its growth.

The injectant was supplied to the mixing layer from a series of holes drilled in the supply tube for each compartment. These holes were arranged so that the gas distribution from the supply tube increased linearly with distance back from the tip cone. That is, equal amounts of gas were supplied per unit cone area.

Gas Supply

During the test program, nitrogen, helium, and sulphur hexafluoride were injected into the conical dead-air region. The gas supply rate to the three forward compartments was measured by a flowmeter system comprised of three Fischer-Porter Flowrators and associated plumbing. The gas supply system is shown in Fig. 4.

Nitrogen was obtained from laboratory supply tanks. Helium was delivered from an 80,000 SCF tank truck. Sulphur hexafluoride was available from a bank of cylinders containing liquid SF_6.

Wind Tunnel

The test program was conducted in two closed circuit wind tunnel facilities at the NASA Jet Propulsion Laboratory. Tests were conducted at three Mach numbers in the 21-inch hypersonic wind tunnel (HWT) and at two Mach numbers in the 20-inch supersonic wind tunnel (SWT). The range of test conditions (Reynolds number versus Mach number) are shown in Fig. 5. The range of test variables are given in Table I. Both tunnel stagnation temperature and pressure were varied when possible. The tunnel running conditions were fixed by the heater limit for maximum T_t and by the condensation limit for minimum T_t.

Flow Patterns

Figure 6 is a schlieren photograph of a run in which air was injected at $M_t = 4.0$. The mixing layer is clearly visible in the lower half of the picture and the beginning of transition is indicated by the change from a thin line to a fuzzy region growing more rapidly. Transition does not appear to be complete until the flow passes the first disc, where the rate of spread of the mixing layer reaches its final value.

TABLE I

WIND TUNNEL TEST PARAMETERS

TUNNEL	M_T	M_C	T_0(°F) RANGE	P_0(cm) RANGE	T_i/T_e RANGE	GAS	DISC SIZE
S_{W_T}	1.48	1.1	95	35- 40	.86	N, H	M
	2.61	2.1	100	36- 73	.60- .64	N, H, SF_6	S, M, L
H_{W_T}	4.04	3.0	340-820	110-215	.52-1.00	N, H, SF_6	S, M
	6.07	4.0	335-690	900	.41- .57	N, H, SF_6	S, M, L
	9.63	4.8	1195	3300	.58- .60	N	S, M

Because the displacement effect on the outer flow is much larger for the turbulent layer than for the laminar one, the effective cone angle changes over the transition region. The photograph shows weak shock waves emanating from the region around the first disc, where the corner in the effective cone surface is concentrated. This has implications for the data reduction in that the flow is not strictly conical or self-similar all the way from the tip.

The effect of the initial laminar run on the entrainment coefficient can be shown to be small, both by a theoretical estimate and by comparing the data from the second and third model compartments.

The discontinuity in cone angle, of course, implies a discontinuity in the flow conditions external to the mixing layer. This is small enough, however, that the relationship between pressure and stream density in the external flow is still locally valid. In other words, data from the second and third compartments can be reduced as if the flow were conical all the way to the tip.

Tunnel Contamination

Because both wind tunnels were closed circuit facilities, the foreign gas injectant served to contaminate the flow. Exchange air was pumped into the tunnel to replace the tunnel flow lost from the high pressure sections. The exchange air was the only means of controlling the level of the foreign gas during the test. Samples of wind tunnel air were taken after many minutes of injecting the mixing gas and were analyzed for foreign gas content. The steady state level of the helium was found to be 3.3 percent by mass and the level of the SF_6 was measured to be 34.6 percent by mass. The effect of helium contamination on tunnel performance was checked and found to be negligible whereas the tunnel operation was seriously affected by the SF_6. Consequently the SF_6 data was not reduced.

Effects of Changes in Disc Sizes

The purpose of constructing the model so as to allow for the use of three different disc sizes was to make it possible to obtain high sensitivity in the detection of axial flow without interfering with the natural development of the mixing layer. The largest disc size which avoids this interference is the optimum, since it confines the flow across any disc to the smallest allowable area. In the absence of any previous use of this technique, a trial-and-error procedure was the only one available for seeking such an optimum.

It was found in the wind-tunnel tests that all three disc sizes provided adequate sensitivity. With all three it was possible to detect small enough axial flows that the individual gas supplies could be repeatedly set to within the least count of the flowmeters.

As for the lack of interference with the natural entrainment process, it was found in tests with air injection that data obtained with the small and medium discs agreed whereas those obtained with the large discs were significantly different. This is illustrated in Fig. 10 in which all the data are plotted in terms of the correlating function derived below. Also evident from this figure is the apparent interference of medium discs with natural entrainment when helium was injected at the two lowest Mach numbers.

In view of the data correlation shown in Fig. 10 between results obtained with the small and medium discs, it may be concluded that these discs did not interfere with natural entrainment and that the data obtained with them correctly describes the behavior of free turbulent mixing layers.

Estimate of Accuracy

For each data point obtained in this investigation it was necessary to match the gas supplied to each compartment to the amount entrained by the mixing layer. At a number of test conditions a measurement of the uncertainty involved in this matching procedure was obtained by repeating it several times without changing the test conditions. It was found to be of the order of ± 3 percent with no significant variation over the range of experimental conditions.

The accuracy of the computed entrainment coefficients depends on the accuracies of the measurements of both mass flow, $\dot{m}$, and external mass velocity, $\rho_e u_e$.

The manufacturer's specification of the flowmeter accuracy is ± 2 percent of full scale, which amounts to ± 4 percent of the average scale readings in these tests.

The external mass velocity is computed from the ratio of the pressure measured in the separated region, p_c, to the tunnel static pressure, p_∞. The

inaccuracy in the former pressure is estimated to be about $\pm 3\%$ which is much larger than that in the tunnel pressure. It can be seen from Fig. 7 that the conical-flow equations predict a much smaller value for the resulting inaccuracy in mass velocity, $\rho_e u_e$ less than $\pm 1\%$. However, as mentioned above in the discussion of flow patterns, the flow is not strictly conical, due to the initial laminar flow in the mixing layer. The estimated error in assuming a true conical flow increases with Mach number from a negligibly small value at M = 1.5 to about $\pm 8\%$ at M = 9.5.

A further source of error in the quoted results is the uncertainty in the transverse curvature correction, discussed below. Estimating this to be possibly as large as 50% of the correction yields errors of the order of 10% at M = 1.5 and of 6% at M = 9.5.

The density, ρ_e, in the stream adjacent to the mixing layer is computed, like the external mass velocity, $\rho_e u_e$, from a pressure measurement in the separated region. As illustrated in Fig. 7 it is affected more strongly than the stream density by errors in p_c/p_∞. The fractional uncertainty in density ratio is of the order of the uncertainty in the pressure measurement or about $\pm 3\%$. The uncertainty in the measurement of the temperature at the inner edge of the mixing layer, T_i, is estimated at about $\pm 1\%$, while the possible error, due to imperfect mixing, is estimated at about $\pm 2\%$.

These various errors and uncertainties are summarized in Table II on the following page.

The uncertainty in the parameter plotted in Fig. 10 is thus estimated to be roughly $\pm 5\%$, which is consistent with the scatter in the data at any fixed Mach number.

The possible inaccuracy in the correlated data, after the uncertainties have been averaged out, is thus estimated to be roughly $\pm 10\%$. This is approximately equal to the inaccuracies found in the more conventional method of measuring mixing layer growth, using profile measurements.

DATA REDUCTION

Definition of Entrainment Coefficient

The rate, $\dot{m}$, at which gas was entrained into the mixing layer from the dead air region was measured directly by the flowmeter system, for

the first three compartments of the model. The mass entrained per unit surface area was computed as

$$G = \frac{\dot{m}}{A} \tag{1}$$

where A denotes the lateral area of the conical frustum included between the appropriate pair of discs. The cone angle used in the computation of A was the basic 16° defined by the tangent from the spike tip to the shoulder of the model face.

A non-dimensional measured entrainment coefficient, c_q', was defined by dividing G by the mass velocity, $\rho_e u_e$, of the supersonic flow at the outer edge of the mixing layer.

$$c_q' = \frac{G}{\rho_e u_e} \tag{2}$$

TABLE II

	ERROR		UNCERTAINTY
	$M_T \approx 1.5$	$M_T \approx 9.5$	All M
Matching gas supply to mixing layer scavenging			± 3%
Flowmeter measurement of $\dot{m}$	± 4%	± 4%	
External mass velocity	< 1%	± 4%	± 1%
Transverse Curvature Correction	± 10%	± 6%	
Entrainment coefficient C_q	± 11%		± 3%
External temperature T_e	< 1%	± 4%	± 3%
Internal temperature T_i	± 2%	± 2%	± 1%
CORRELATION PARAMETER OF FORMULA (12)	± 11%	± 9%	± 5%

Computation of the Flow Properties at the Outer Edge of the Mixing Layer

The mass velocity $\rho_e u_e$ along the outer edge of the mixing layer was determined by measuring the cone static pressure. A unique relation exists for each free-stream Mach number between the ratio of properties at the edge of a conical surface and the free stream properties. An example of this is given in Fig. 7 where the ratio of cone to free-stream density is presented in terms of the pressure ratio p_c/p_∞.

The static-temperature ratio T_e/T_∞ is also uniquely determined by the pressure ratio p_c/p_∞ and this relationship is also illustrated in Fig. 7. Since the total temperature is conserved across the conical shock, the Mach number at the outer edge, M_e, may be computed from the ratio T_e/T_{te}.

Note that all these computations of flow properties, external to the mixing layer, do not require any assumption about the effective cone angle. The various ratios are determined strictly from a measurement of the cone pressure and a knowledge of the free-stream Mach number. The effective cone angle can be derived, also.

The free-stream flow properties were determined from the tunnel calibration and pressure and temperature measurements in the stilling section for each run.

Transverse Curvature Correction

It is shown in Appendix A that the equations of motion for a thick conical mixing layer can be reduced to the same differential equation as those for two-dimensional flow. There is, however, a difference in the expressions for the entrainment coefficient. In terms of the solution of the basic differential equation (35) the entrainment coefficient in a two-dimensional flow is

$$c_q = \frac{-f(-\infty)}{2\sigma} \tag{3}$$

whereas in the conical flow it is

$$c_q' = -\frac{y_o}{y_i}\,\frac{f(-\infty)}{\sigma'} \tag{4}$$

It is also shown that an application of Prandtl's (Ref. 5) basic formula for the eddy viscosity to both mixing layers leads to the relation

$$\sigma' = 2\,\sigma \tag{5}$$

and thus defines the ratio of entrainment coefficients in the two flows as

$$\frac{c_q}{c_q'} = \frac{y_i}{y_o} \tag{6}$$

As defined in Appendix A, y_i and y_o are the radii of the inner and mean surfaces of the mixing layer.[1] In a conical flow their ratio is constant and approximately equal to

$$1/\left(1 + \frac{b}{2y_i}\right) \tag{7}$$

where b is the width of the layer. In this flow

$$b \approx \frac{x\delta}{\sigma'} \text{ and } c'_q \approx \frac{f(-\infty)}{\sigma} \tag{8}$$

so that

$$1 + \frac{b}{2y_i} \approx 1 + 0.87\,B\,c_q' \tag{9}$$

in terms of the shape parameter B defined in equation (48). The value of B depends on the Mach number of the external flow and the temperature ratio across the layer and is given for air and helium injection by the formulas (49) and (50).

All the measured values of c_q' have been corrected for this transverse curvature effect by dividing them by $(1 + 0.87\,B\,c_q')$. The results quoted in the following discussion thus apply to two-dimensional flows. All previous measurements quoted in the literature are for two-dimensional flows and thus directly comparable.

EXPERIMENTAL RESULTS

Variation of c_q with Temperature Ratio Across the Mixing Layer

In Fig. 8 the entrainment coefficient c_q has been plotted versus the temperature ratio across the mixing layer T_e/T_i. There are three sets of data, each one corresponding to a fixed value of the Mach number. Two of these sets are for air entrainment and the other for helium.

The straight lines shown represent the best fit which can be obtained keeping the slopes equal. They represent expressions of the form

$$c_q \propto (T_e/T_i)^{0.4} \tag{10}$$

and fit the data quite well.

There is no systematic influence of Reynolds number, which varies over a range of about 3 to 1, on the results. None is expected for a fully developed turbulent mixing layer.

Correlation of all the Data for Air and Helium

In Fig. 9 the variation of c_q with Mach number has been isolated from the effects of temperature ratio by plotting $c_q (T_i/T_e)^{0.4}$ versus the Mach-number parameter T_e/T_{te}. All the data for air and helium are represented.

The best straight-line fit to the air data is

$$c_q = 0.049 \left[\frac{T_e}{T_i}\right]^{0.4} \left[\frac{T_e}{T_{te}}\right]^{0.67} \tag{11}$$

The helium data can be fitted with a parallel straight line displaced by an amount corresponding to the ratio

$$\left[\frac{\text{molecular weight of helium}}{\text{molecular weight of air}}\right]^{0.4}.$$

This means that all the data for both gases can be represented by the formula

$$c_q = 0.049 \left[\left(\frac{\rho_i}{\rho_e} \right)^{-0.4} \left(1 + \frac{\gamma - 1}{2} M_e^2 \right) \right]^{-0.67} \qquad (12)$$

The degree to which this expression fits the data is illustrated in Fig. 10 where the parameter

$$c_q \left[\left(\frac{\rho_e}{\rho_i} \right)^{-0.4} \left(1 + \frac{\gamma - 1}{2} M_e^2 \right) \right]^{0.67}$$

has been plotted versus Mach number. Except for some measurements obtained with discs which were too large, all the data fall within ± 10 % of the constant 0.049.

REVIEW OF MIXING LAYER THEORY

Basic Equations

The following assumptions may be made in the theoretical investigation of the particular class of mixing layers of interest in the present research:

(a) zero pressure gradient along the layer

(b) zero velocity along the layer at the inner edge

(c) non-reacting perfect gases

(d) turbulent Prandtl and Lewis numbers equal to unity

Expressing the turbulent terms in terms of the eddy-viscosity concept, we may write the governing equations for two-dimensional flow as follows:

$$\frac{\partial}{\partial x} (\rho u) + \frac{\partial}{\partial y} (\rho v) = 0 \qquad \text{(continuity)} \qquad (13a)$$

$$\rho u \frac{\partial u}{\partial x} + \rho v \frac{\partial u}{\partial y} = \frac{\partial}{\partial y} \left(\rho \epsilon \frac{\partial u}{\partial y} \right) \qquad \text{(momentum)} \qquad (13b)$$

$$\rho u \frac{\partial c}{\partial x} + \rho v \frac{\partial c}{\partial y} = \frac{\partial}{\partial y} \left(\rho \epsilon \frac{\partial c}{\partial y} \right) \qquad \text{(diffusion)} \qquad (13c)$$

$$\rho u \frac{\partial H}{\partial x} + \rho v \frac{\partial H}{\partial y} = \frac{\partial}{\partial y} \left(\rho \epsilon \frac{\partial H}{\partial y} \right) \qquad \text{(energy)} \qquad (13d)$$

Similar equations for axisymmetric flow are discussed in Appendix B.

Solutions of the Diffusion and Energy Equations

Inspection of the last three of the set of equations above shows that c and H must be linear functions of u. These functions must be written to satisfy the boundary conditions;

at the inner edge

$$u = 0 \qquad c = 1 \qquad h = H_i = c_{p_i} T_i \qquad (14)$$

at the outer edge

$$u = u_e \qquad c = 0 \qquad H = H_e = c_{p_e} T_e \left(1 + \frac{\gamma - 1}{2} M_e^2\right) \qquad (15)$$

Therefore,

$$c = 1 - \frac{u}{u_e} \qquad (16)$$

$$H = H_i + (H_e - H_i) \frac{u}{u_e} \qquad (17)$$

Noting that $H = h + 1/2\, u^2$, the static enthalpy profile may be written

$$\frac{h}{h_e} = \frac{h_i}{h_e} + \left(1 - \frac{h_i}{h_e} + \frac{\gamma - 1}{2} M_e^2\right) \frac{u}{u_e} - \frac{\gamma - 1}{2} M_e^2 \left(\frac{u}{u_e}\right)^2 \qquad (18)$$

The molecular weight and specific heat of the binary mixture are

$$\frac{c_p}{c_{p_e}} = 1 + \frac{c_{p_i} - c_{p_e}}{c_{p_e}} \quad c = 1 + \frac{c_{p_i} - c_{p_e}}{c_{p_e}} \left[1 - \frac{u}{u_e} \right] \tag{19}$$

and

$$\frac{m_e}{m} = 1 + \frac{m_e - m_i}{m_i} \quad c = 1 + \frac{m_e - m_i}{m_i} \left[1 - \frac{u}{u_e} \right] \tag{20}$$

Writing

$$\Delta c_p^* = \frac{c_{p_i} - c_{p_e}}{c_{p_e}} \tag{21}$$

and

$$\Delta m^* = \frac{m_e - m_i}{m_i} \tag{22}$$

we may express the density ratio

$$\rho^* = \frac{\rho}{\rho_e} = \frac{R_e T_e}{R T} = \frac{m}{m_e} \frac{c_p}{c_{p_e}} \frac{h_e}{h} = \tag{23}$$

$$\frac{1 + \Delta c_p^* (1 - u^*)}{\left[\frac{c_{p_i} T_i}{c_{p_e} T_e} + \left[1 - \frac{c_{p_i} T_i}{c_{p_e} T_e} + \frac{\gamma - 1}{2} M_e^2 \right] u^* - \frac{\gamma - 1}{2} M_e^2 u^{*2} \right] \left[1 + \Delta m^* (1 - u^*) \right]}$$

where $u^* = u/u_e$.

Eddy Viscosity Formulas

Before the momentum equation can be integrated to obtain the velocity profile, the variation of ϵ, the kinematic eddy viscosity coefficient along and across the layer must be known. For incompressible flow, Prandtl's (Ref. 5) formula

$$\epsilon = k b u_e \tag{24}$$

is generally accepted. Here b is a measure of the width of the layer and k is a universal constant. Since, as will be shown later, the growth of the layer is linear in x, this may also be written

$$\epsilon = \epsilon_0 u_e x \tag{25}$$

The variation of ϵ across the mixing layer, at a fixed value of x, is nil.

In compressible flows, where the density varies across the layer, it has been suggested that ϵ may also vary. At least three formulas have been suggested, which may be written

$$\epsilon = \epsilon_0 u_e \left[\frac{\rho_e}{\rho} \right]^N X \tag{26}$$

with

$$N = 0, 1, 2$$

$N = 0$ preserves the invariance of ϵ across the layer and has been used by Crane (Ref. 6) and others.

$N = 1$ corresponds to an invariant dynamic viscosity coefficient and has been suggested by Ferri (Ref. 7).

$N = 2$ allows a convenient transformation by which the equations for compressible flow may be reduced to incompressible form and has been suggested by Ting and Libby (Ref. 8).

Transformation of the Equations of Continuity and Momentum to an Ordinary Differential Equation

The pair of equations (13a) and (13b) may be reduced to an ordinary differential equation, defining a self-similar flow, as follows.

The new independent variable is

$$\eta = \sigma \frac{y}{x} \tag{27}$$

where σ is an undertermined spreading parameter. The rate of growth of the layer is thus linear with x.

The new dependent variable is a reduced stream function

$$f = \frac{2}{\rho_e u_e} \frac{\sigma \psi}{x} \tag{28}$$

where

$$\rho u = \frac{\partial \psi}{\partial y} \text{ and } \rho v = \frac{\partial \psi}{\partial x} \tag{29}$$

so that the continuity equation is satisfied.

The velocity components in terms of the new variables are given by

$$\rho u = \frac{\rho_e u_e}{2} \frac{df}{d\eta} \tag{30}$$

$$\rho v = \frac{\rho_e u_e}{2\sigma} \left(\eta \frac{df}{d\eta} - f \right) \tag{31}$$

and the momentum equation may be written

$$f \frac{d}{d\eta} \left[\frac{\rho_e}{\rho} \frac{df}{d\eta} \right] + 2 k \delta \sigma \frac{d}{d\eta} \left[\left[\frac{\rho_e}{\rho} \right]^{N-1} \frac{d}{d\eta} \left[\frac{\rho_e}{\rho} \frac{df}{d\eta} \right] \right] = 0 \tag{32}$$

where δ defines the (constant) width of the layer in the similarity variable η

$$\delta = \frac{\sigma b}{x} \tag{33}$$

It is convenient to choose σ so as to obtain an equation which is free of all empirical constants. If

$$\sigma = \frac{1}{4k\delta} \tag{34}$$

the momentum equation becomes

$$2f \frac{d}{d\eta} \left[\frac{\rho_e}{\rho} \frac{df}{d\eta} \right] + \frac{d}{d\eta} \left[\left(\frac{\rho_e}{\rho} \right)^{N-1} \frac{d}{d\eta} \left[\frac{\rho_e}{\rho} \frac{df}{d\eta} \right] \right] = 0 \tag{35}$$

which for incompressible flow reduces to

$$2 ff'' + f''' = 0 \tag{36}$$

This last equation has been solved by Görtler (Ref. 9) and yields the standard velocity profile for the turbulent mixing layer in incompressible flow.

The boundary conditions at the outer and inner edges of the layer are

$$f'(\infty) = 2 \qquad f'(-\infty) = 0 \tag{37}$$

A third boundary condition is required which serves to locate the origin of the coordinate system. We choose here to locate it on the dividing streamline so that

$$f(0) = 0 \tag{38}$$

Integration of the Momentum Equation

The momentum equation (35) may be integrated for all values of N by an iterative procedure due to Chapman (Ref. 4).

The equation is written in the form

$$\frac{\frac{d}{d\eta}\left[\left(\frac{\rho_e}{\rho}\right)^{N-1}\frac{d}{d\eta}\left(\frac{\rho_e}{\rho}f'\right)\right]}{\left(\frac{\rho_e}{\rho}\right)^{N-1}\frac{d}{d\eta}\left(\frac{\rho_e}{\rho}f'\right)} = -2\left(\frac{\rho}{\rho_e}\right)^{N-1} f \tag{39}$$

which integrates immediately to yield

$$\left(\frac{\rho_e}{\rho}\right)^{N-1}\frac{d}{d\eta}\left(\frac{\rho_e}{\rho}f'\right) = 2\,c_1\,F \tag{40}$$

where

$$F = \exp\left[-\int_0^\eta 2\,(\rho^*)^{N-1}\,f\,d\eta\right] \tag{41}$$

A second integration yields

$$u^* = \frac{1}{2}\,\frac{\rho_e}{\rho}f' = c_1\int_0^\eta (\rho^*)^{N-1}\,F\,d\eta + c_2 \tag{42}$$

The solution is obtained by starting with an assumed profile $u_0^*(\eta)$ from which

$$f = 2\int_0^\eta \rho^*\,u^*\,d\eta \tag{43}$$

can be obtained directly, using the formula (23) for $\rho^*(u^*)$. This automatically satisfies $f(0) = 0$. The first approximation to the correct profile is then computed as

$$u_1(\eta) = c_1\int_0^\eta (\rho^*)^{N-1}\exp\left[-4\int_0^\eta (\rho^*)^{N-1}\int_0^\eta \rho^* u_0^*\,d\eta\,d\eta\right]d\eta + c_2 \tag{44}$$

with c_1 and c_2 calculated to give

$$u^*(\infty) = 1 \qquad u^*(-\infty) = 0 \tag{45}$$

This process is repeated starting with $u_1^*(\eta)$ and each successive approximation until the difference between two successive profiles becomes negligible.

Solutions for the case N = 2 can also be obtained by simple quadratures from the incompressible solution, using the transformation of Ting and Libby (Ref. 8).

The conditions required to specify a solution all appear in the formula (23) for ρ^*. They are

a) Mach number of the external flow M_e

b) temperature ratio across the layer T_i / T_e

c) specific heat ratio of the two gases Δc_p^*

d) molecular weight ratio of the two gases Δm^*

Solutions have been obtained on an IBM 7090 computer for a number of sets of these conditions covering the range of the experiments.

Results: Velocity Profiles

The profile shapes obtained using different values of the exponent N in the eddy-viscosity formula (26) exhibit increasing differences as the Mach number increases and compressibility effects become pronounced. On the basis of these differences particular values of N may be accepted or rejected as being compatible with experimental evidence.

In fig. 11 the velocity profiles calculated with N = 0, 1, 2 are compared with the measurements of Chrisman (Ref. 10) taken at $M \approx 2.76$ in an isoenergetic flow of air into air. This is the highest value of M for which data is known by the authors to be available.

In order to compare the various profile shapes they have been drawn to a common scale which corresponds to that of the standard solution for incompressible flow. Scaling has been accomplished by applying a linear transformation.

$$\bar{\eta} = a\,\eta + b \tag{46}$$

to the η-coordinates of the various solutions for M = 2.76. The coefficients have been determined by plotting η (M = 2.76) versus η (M = 0) for equal values of u/u_e. A linear fit to the points in the region $0.4 < u/u_e < 0.7$ then was used to fix a and b.

Referring to Fig. 11 we note that the compressibility effects on profile shape are not very large at this Mach number. The experimental points favor the profile corresponding to N = 0 but fit the incompressible profile almost equally well. The profile for N = 2 is far enough from the data that the corresponding eddy viscosity formula of Ting and Libby (Ref. 8)

$$\epsilon = \epsilon_0 u_e \left[\frac{\rho_e}{\rho}\right]^2 x \qquad (47)$$

must be regarded as inconsistent with these measurements.

Results: Shape Parameters

Further discussion of compressibility effects on mixing-layer profiles is most conveniently accomplished by introducing a suitable shape parameter, since an atlas of profiles for various values of M_e and T_i / T_e would be cumbersome; even more so if binary mixing were to be considered.

A choice of shape parameter which is useful in comparing our data with other measurements is

$$B = \frac{\rho_e u_e}{\rho_i v_i} \frac{db}{dx} = -\frac{2\delta}{f(-\infty)} \qquad (48)$$

This parameter essentially describes how fast the mixing layer must grow in order to absorb the rate of fluid entrainment. Its value depends on M_e, T_i/T_e, and the molecular weight and specific-heat ratios of the two gases which are mixing across the shear layer.

Because the approach of the velocity profile to zero at the inner edge and u_e at the outer edge is asymptotic, the definition of the width b, is somewhat arbitrary. The choice which has been made here locates the edges at

$$\frac{u}{u_e} = 0.05 \text{ and } \frac{u}{u_e} = 0.95$$

The spacing on the η scale between these two profile points defines δ for any solution of the equations of motion.

Values of B have been computed from solutions of the differential equation (35) with both air and helium as the scavenged gas. The ranges of Mach number and temperature ratio covered are somewhat larger than those of the experiments. The values obtained with N = 0 and N = 1 were

found to agree quite well with each other whereas those for N = 2 were significantly different. Because of this and the profile-shape results, illustrated in Fig. 11, only the values for N = 0 and N = 1 are presented.

For air blowing over air the results of about 20 solutions have been correlated within ± 5 percent by the formula

$$B = 5.74 \left[\frac{T_i}{T_e} \right]^{0.51} \left[\frac{T_{te}}{T_e} \right]^{0.27} \tag{49}$$

and this result is plotted in Fig. 12, illustrating agreement of the solutions for N = 0 and N = 1.

For air blowing over helium the results of about 20 solutions have been correlated within ± 10 percent by the formula.

$$B = 16.2 \left[\frac{T_i}{T_e} \right]^{0.45} \left[\frac{T_{te}}{T_e} \right]^{-0.27} \tag{50}$$

COMPARISON OF RESULTS WITH OTHER MEASUREMENTS

All the other data on turbulent mixing layers have been obtained by measuring profiles; velocity profiles have been measured with pitot-static tubes; and density profiles have been measured with interferometers. These profiles are then fitted to theoretical profiles and the scaling factor is used to determine the spreading parameter σ. In order to compare these results with ours we have developed a method for determining values of σ from measurements of the entrainment coefficient c_q.

Spreading Parameters Determined from Profiles

The common practice in deducing values of σ from profile measurements is to adjust the scale of the appropriate theoretical curve until the best fit with the data points is obtained.

Rosler (Ref. 11) has shown that equally good results may be obtained by simply measuring the rate of increase of the mixing layer width. If the experimental measurements of b versus x are fitted to a straight line,

$$b = m (x + x_0) \tag{51}$$

the spreading parameter is simply

$$\sigma = \frac{\delta}{m} \tag{52}$$

where δ is the theoretical profile width on the η scale.

The choice of theoretical profile to which the measurements may be referred is somewhat arbitrary. Given the appropriate binary mixture, Mach number, and temperature ratio across the layer, three different values of δ are available from the solutions with N = 0, 1, 2, discussed above. Further, as illustrated in Fig. 11, the solution for incompressible flow can be fitted quite well to measured profiles up to at least $M_e = 3$, so that a fourth value of δ is available. The values of σ quoted in the literature are in fact based on this last choice and are obtained by fitting the measured profiles to the basic theoretical solution for incompressible flow, for which $\delta = 2.56$. To distinguish values of σ referred to this profile from the values which appear in the equations for compressible flow, they will be denoted here by σ^*.

Relation Between Rate of Growth and Entrainment Coefficient

The measurements we have obtained of entrainment coefficients, c_q, imply rates of growth of the various mixing layers which may be calculated by means of the shape parameter, B, defined in equation (48). In any specific case

$$\frac{db}{dx} = B\, c_q \tag{53}$$

where B is evaluated for the appropriate flow conditions. It follows that

$$\sigma^* = \frac{2.56}{B\, c_q} \tag{54}$$

Result for Incompressible Flow

Equation (12), which correlates the results of our measurements, yields for $M_e = 0$ and $T_i/T_e = 1$,

$$c_q = 0.049$$

The corresponding value of σ^* given by (54) is

$$\sigma_0^* = 9$$

The values obtained from velocity-profile measurements range from $\sigma_0^* = 11$ measured by Liepmann and Laufer (Ref. 12) to $\sigma_0^* = 13.5$ measured by Reichardt (Ref. 13). The generally quoted $\sigma_0^* = 12$ has been obtained by fitting the measurements to the older theoretical profile of Tollmien (Ref. 1) which differs slightly from the solution of equation (36).

A possible explanation of these discrepancies lies in the different geometrical situations. Liepmann and Laufer's measurements were obtained in a two-dimensional flow whereas Reichardt's were obtained at the edge of a round jet. There may be a transverse-curvature effect associated with the effectively wider (around the perimeter) low-speed and narrower high-speed region of the mixing layer in the axisymmetric case.

The measurements reported here were also obtained with axially symmetric geometry. The situation was "inside-out" with respect to Reichardt's since fluid was scavenged from the inner side of the mixing layer. It turns out that the value $\sigma_0^* = 9$ obtained here is as much below the two-dimensional $\sigma_0^* = 11$ as Reichardt's $\sigma_0^* = 13.5$ is above it. Since there is no other data on transverse-curvature effects of this kind, and any theory necessarily contains an empirical constant, it is not possible to pursue this discrepancy further.

Results for Compressible Flow

Previously reported measurements of compressibility effects on turbulent mixing-layer growth have been limited to the special case of isoenergetic flow of air into air. Here $T_i/T_e = T_{te}/T_e$ and Equations (11) and (49) may be written

$$c_q = 0.049 \, (T_e/T_{te})^{1.07} \tag{55}$$

$$B = 5.74 \, (T_{te}/T_e)^{0.78} \tag{56}$$

Substitution of these expressions into (54) yields a simple formula for σ^*;

$$\sigma^* = 9.1 \, (T_{te}/T_e)^{0.29} \tag{57}$$

for this special class of flows. In order to isolate the compressibility effects from the uncertainties in the result for incompressible flow the comparison of other data will be made with the function $12\sigma^*/\sigma^*_0$ whose value at M = 0 is the generally quoted $\sigma^* = 12$. A plot of this function versus Mach number is shown in Fig. 13.

Also shown in Fig. 13 are values of σ^* deduced from measurements reported in the literature. The results of Bershader and Pai (Ref. 14) and of Gooderum, Wood, and Brevoort (Ref. 15) were obtained by comparing interferometer measurements with theoretical density profiles and are quoted as published. The result of Chrisman (Ref. 10) has been derived from his measurements of velocity profiles as plotted in Fig. 11. The measurements of Maydew and Reed (Ref. 12) have been reduced to values of σ^* by the method outlined in Appendix G, which allows for the conical growth of the mean surface in the mixing layer as well as the increase in its width.

As shown in Fig. 13, all measurements of σ^* using profile measurements in supersonic flows lie above the curve computed from our measurements of entrainment. No explanation for this discrepancy has been established. Part of the difficulty may be in the translation of the entrainment data into a curve σ^*, which involves a theory as yet unchecked by experiment. The theoretical result for the shape parameter B is plausible because the predictions of the two theories with $N = 0$ and $N = 1$ agree. A conclusive check on the transformation from entrainment to σ^* could only be obtained from a simultaneous measurement of velocity profiles and fluid entrainment.

Finally, Fig. 13 includes a curve which describes the variation of σ^* which can be developed from the special solutions for the mixing layer profiles which apply when $N = 2$. As noted above, the assumption $N = 2$ in the eddy-viscosity formula (26) allows the equations for compressible flow to be reduced to incompressible form by the application of a Howarth-Dorodnitsyn transformation in Appendix D. This transformation is used to develop a very simple formula for the effect of compressibility on c_q, namely

$$c_q = c_{q_0} \, T_e / \sqrt{T_{te} \, T_i} \tag{58}$$

for the injection of air into air.

Now for the particular case of the isoenergetic flow of air into air the variation with Mach number of the shape parameter B obtained from our numerical solution for $N = 2$ is

$$B = 5.87 \left[\frac{T_{te}}{T_e} \right]^{0.75} \tag{59}$$

only slightly different from the result (56). The corresponding result for variation of σ^* is, therefore,

$$\frac{\sigma^*}{\sigma^*_0} = \left[\frac{T_{te}}{T_e}\right]^{0.25} \tag{60}$$

as shown in Fig. 13. The difference from the result (57) based on our measurements is negligible.

CONCLUSIONS

1. A new wind-tunnel technique has been developed by means of which the fluid entrainment rates of turbulent mixing layers may be measured directly.

2. Entrainment of both helium and air over a wide range of conditions may be correlated with only two parameters. One is the Mach number of the external stream and the other is the density ratio across the mixing layer. All the measurements obtained fit the formula.

$$c_q = 0.049 \left[\frac{\rho_i}{\rho_e}\right]^{0.4} \left[1 + \frac{\gamma - 1}{2} M_e^2\right]^{-0.67} \tag{12}$$

within $\pm$ 10 percent.

3. In order to compare direct measurements of fluid entrainment with the measurements of spreading rate found in the literature, some information about the structure of the mixing layer is necessary. It has been shown that the information required may be simply expressed as the value of a shape parameter B, defined by equation (48).

4. Values of B for given flow conditions may be found by integrating the equations of motion for the flow in the turbulent mixing layer. Such integrations have been performed with three different formulas, for the variation of eddy viscosity, across the mixing layer, corresponding to N = 0, 1, and 2 in the expression

$$\epsilon = \epsilon_0 u_e \left[\frac{\rho_e}{\rho}\right]^N X \tag{26}$$

The results obtained with N = 0 and N = 1 agree with each other but differ from those with N = 2. The latter value gives profile shapes which become more inconsistent with measurements as the Mach number is increased; the corresponding values of B have therefore been disregarded. With N = 0 and 1 the results for air and helium taken separately may be correlated by using the same parameters as for the entrainment coefficient c_q.

5. Values of the spreading parameter σ^* for the isoenergetic entrainment of air by air have been computed from the measurements of c_q and the calculations of B. When these are plotted versus Mach number they fall somewhat below most of the measurements reported in the literature.

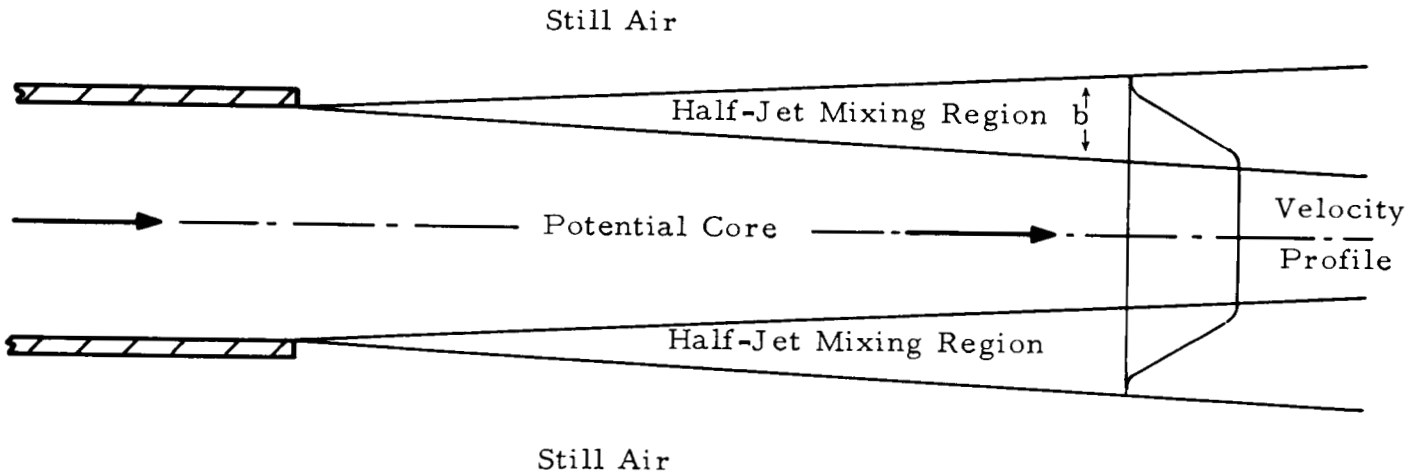

Figure 1. Schematic of half-jet flow.

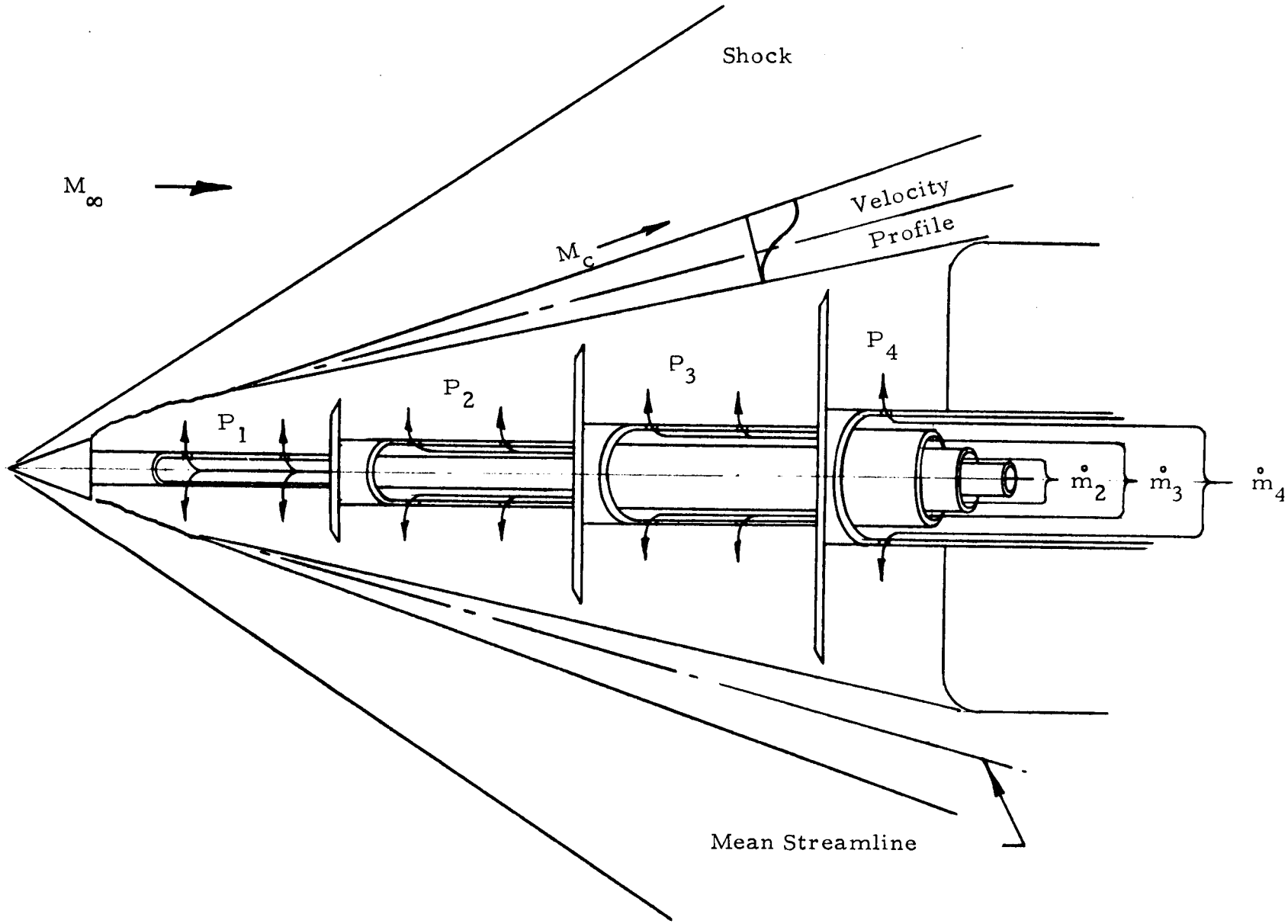

Figure 2. Schematic of measurement technique.

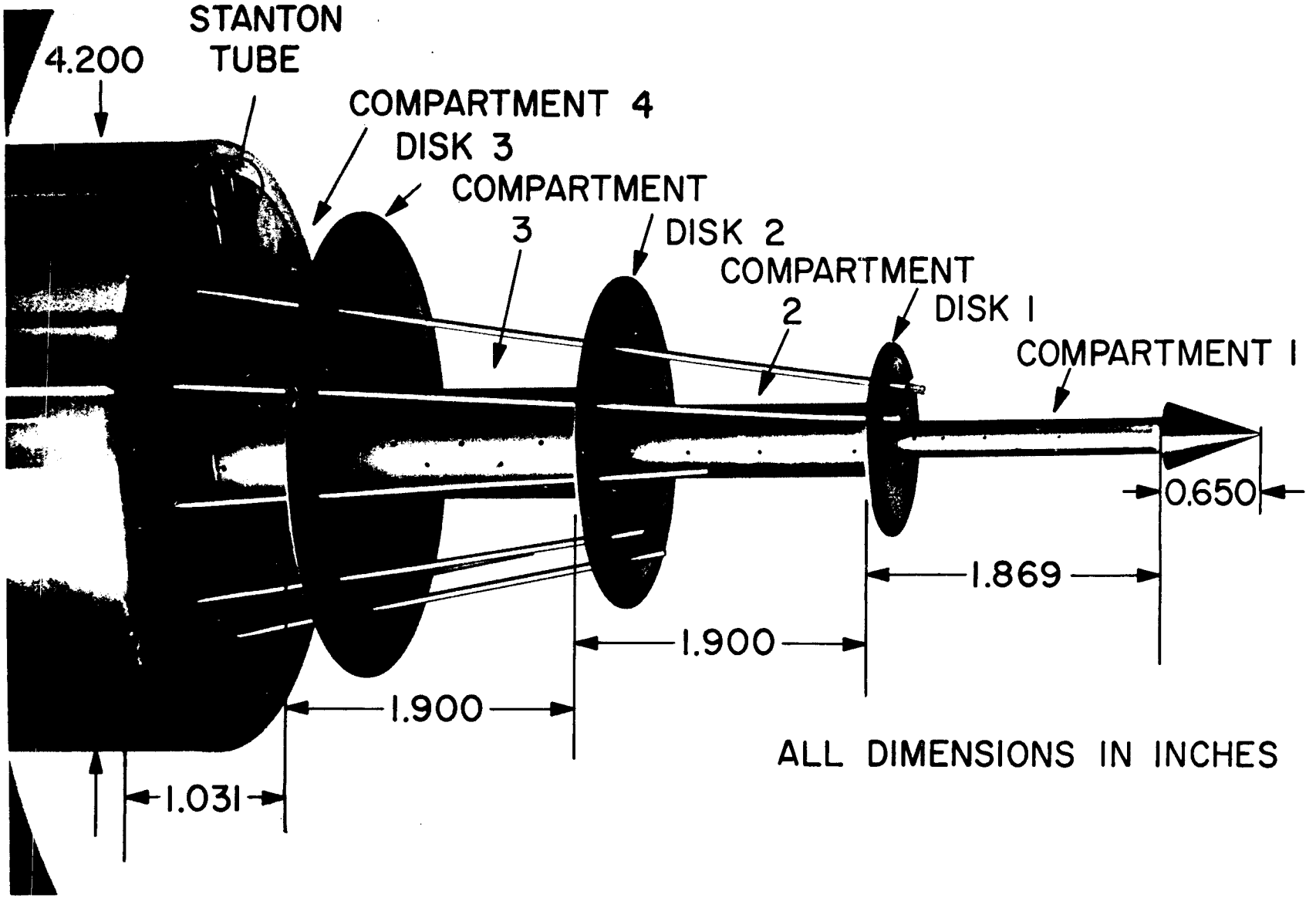

Figure 3. Wind-tunnel model.

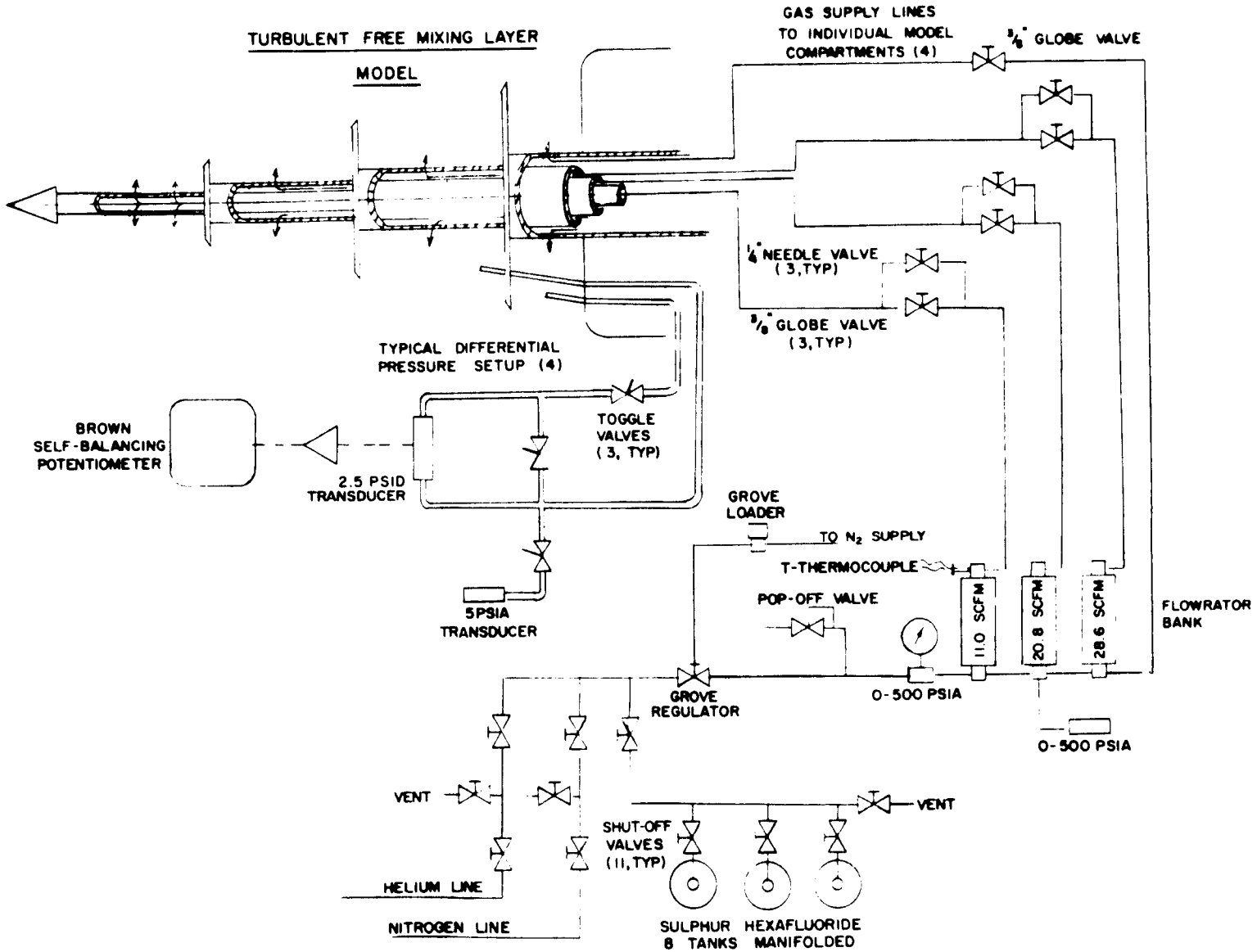

Figure 4. Schematic of gas supply system.

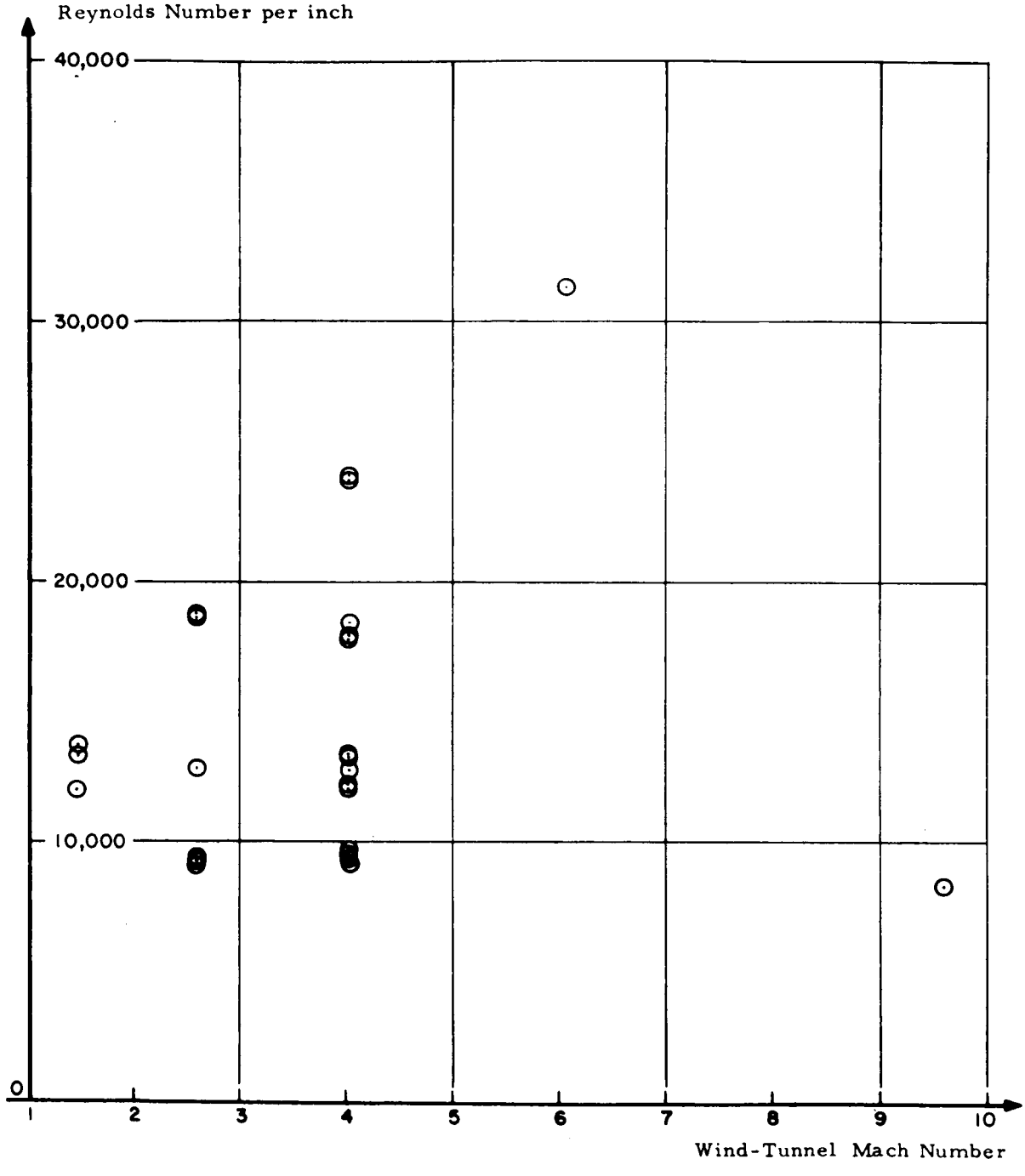

Figure 5. Mach- and Reynolds-number range of the measurements.

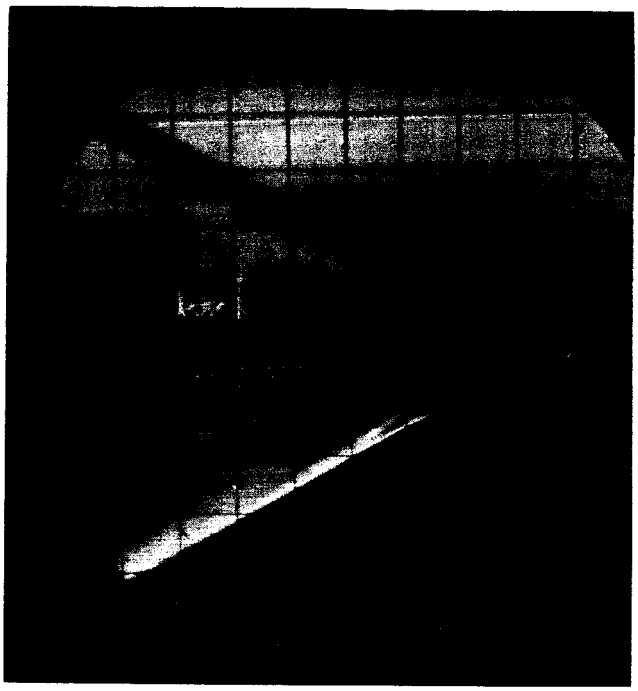

Figure 6. Schlieren photograph of air injection at $M_\infty = 4$.

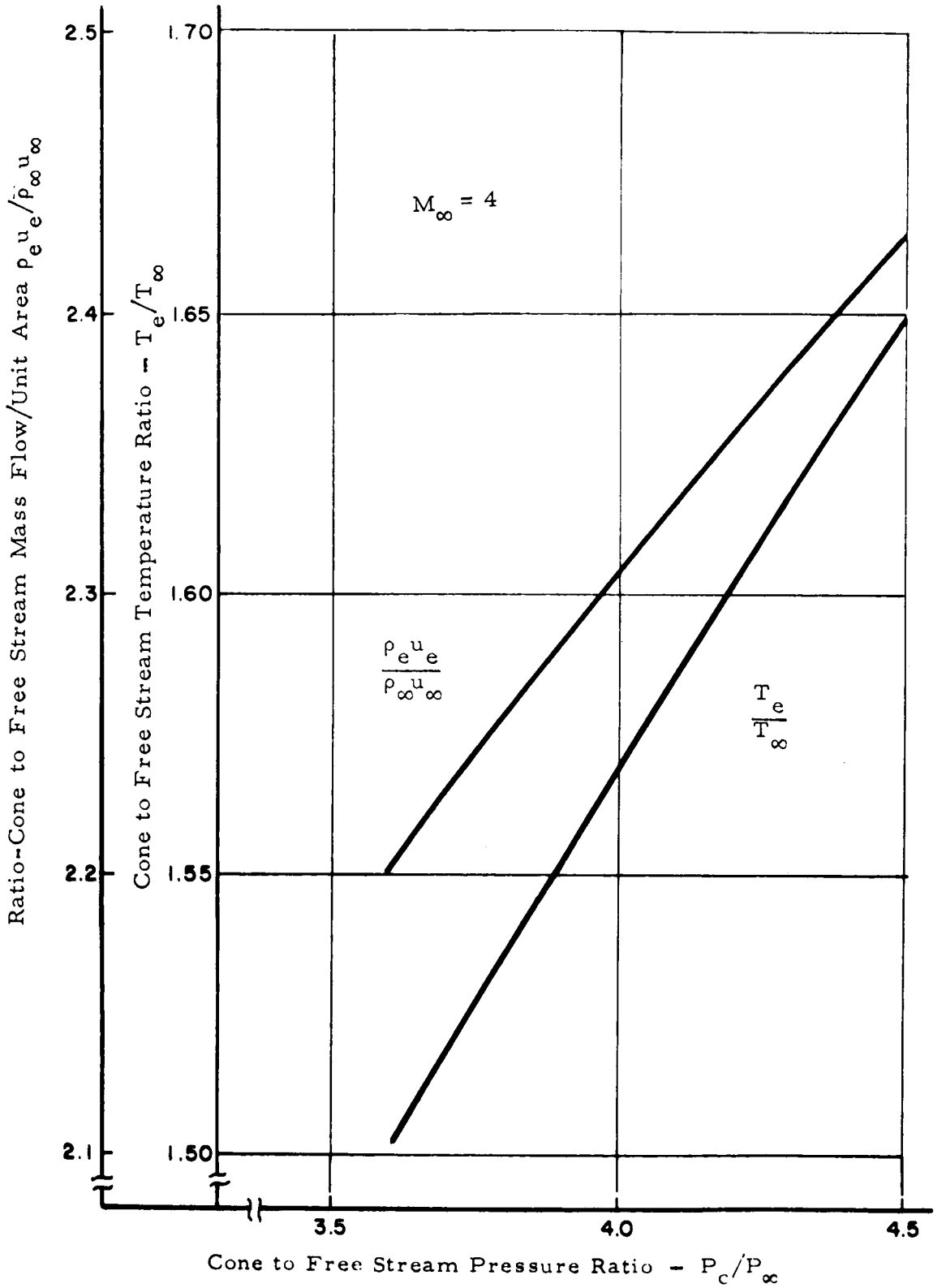

Figure 7. Flow properties at the outer edge of the mixing layer plotted against static pressure in the separated region; $M_\infty = 4.0$.

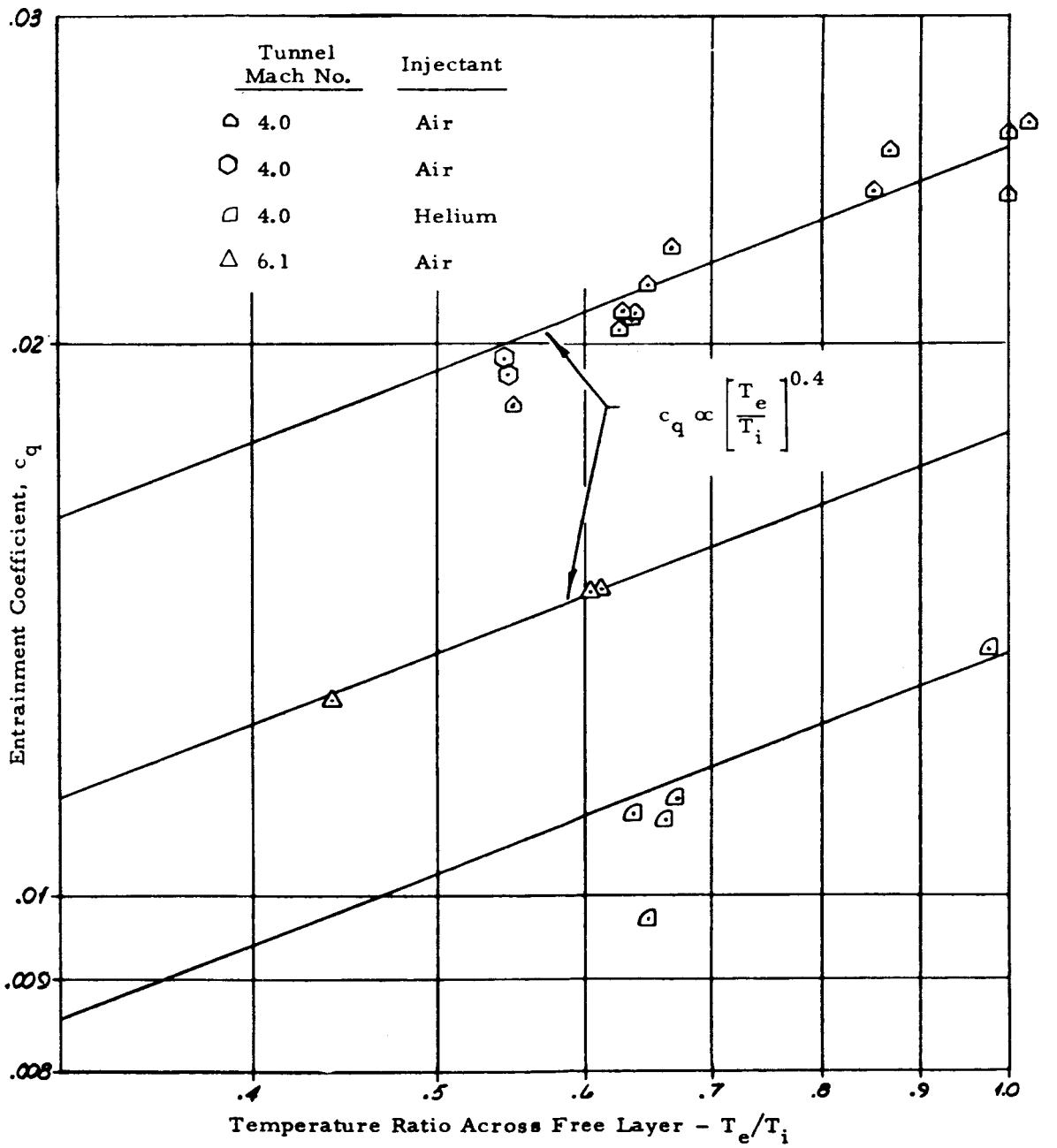

Figure 8. Entrainment coefficient, c_q, plotted against temperature ratio T_e/T_i for fixed values of the Mach number, M_e.

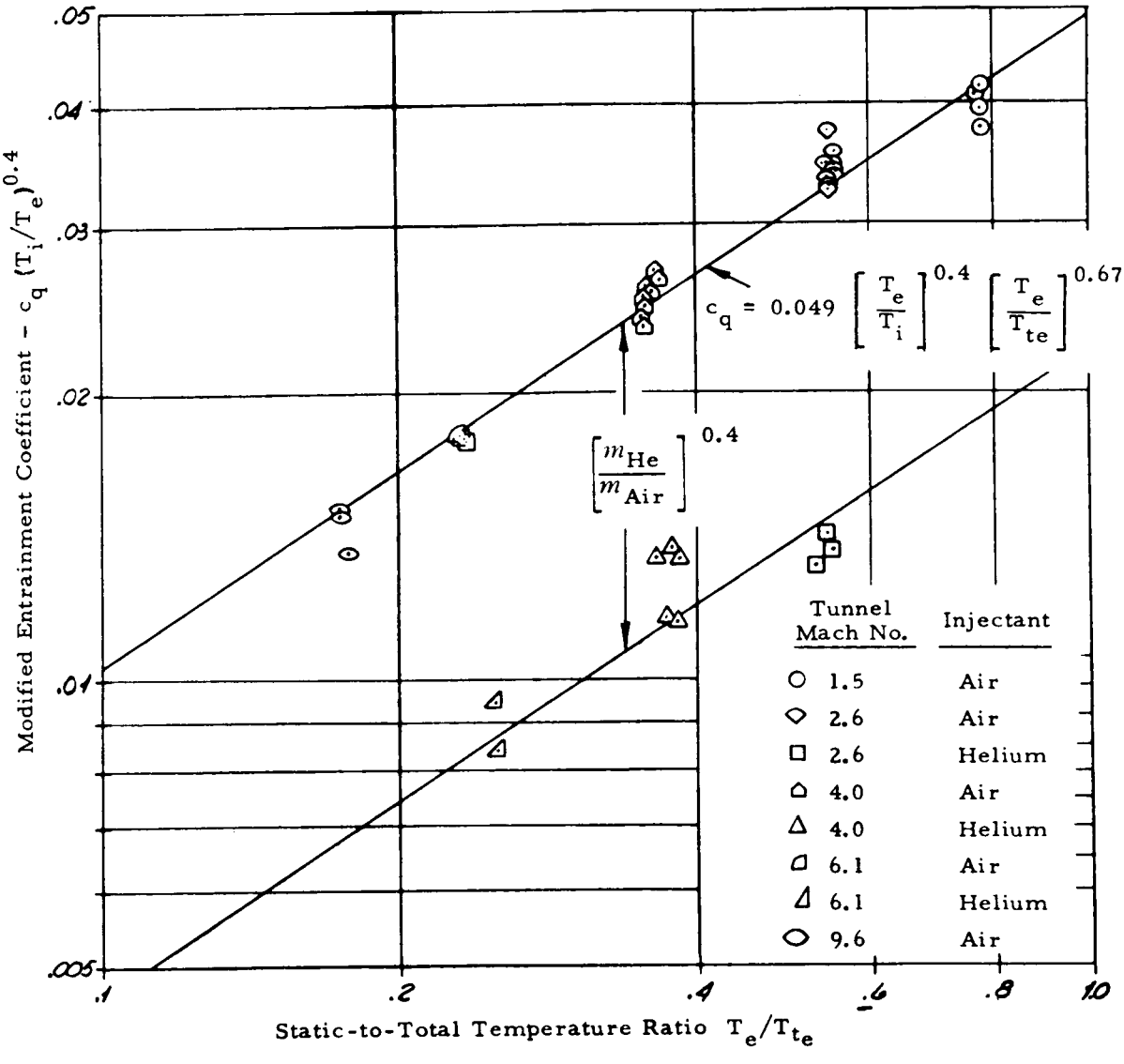

Figure 9. Reduced entrainment coefficient, $c_q(T_i/T_e)^{0.4}$, plotted against the static-to-total temperature ratio, T_e/T_{t_e}, of the external stream.

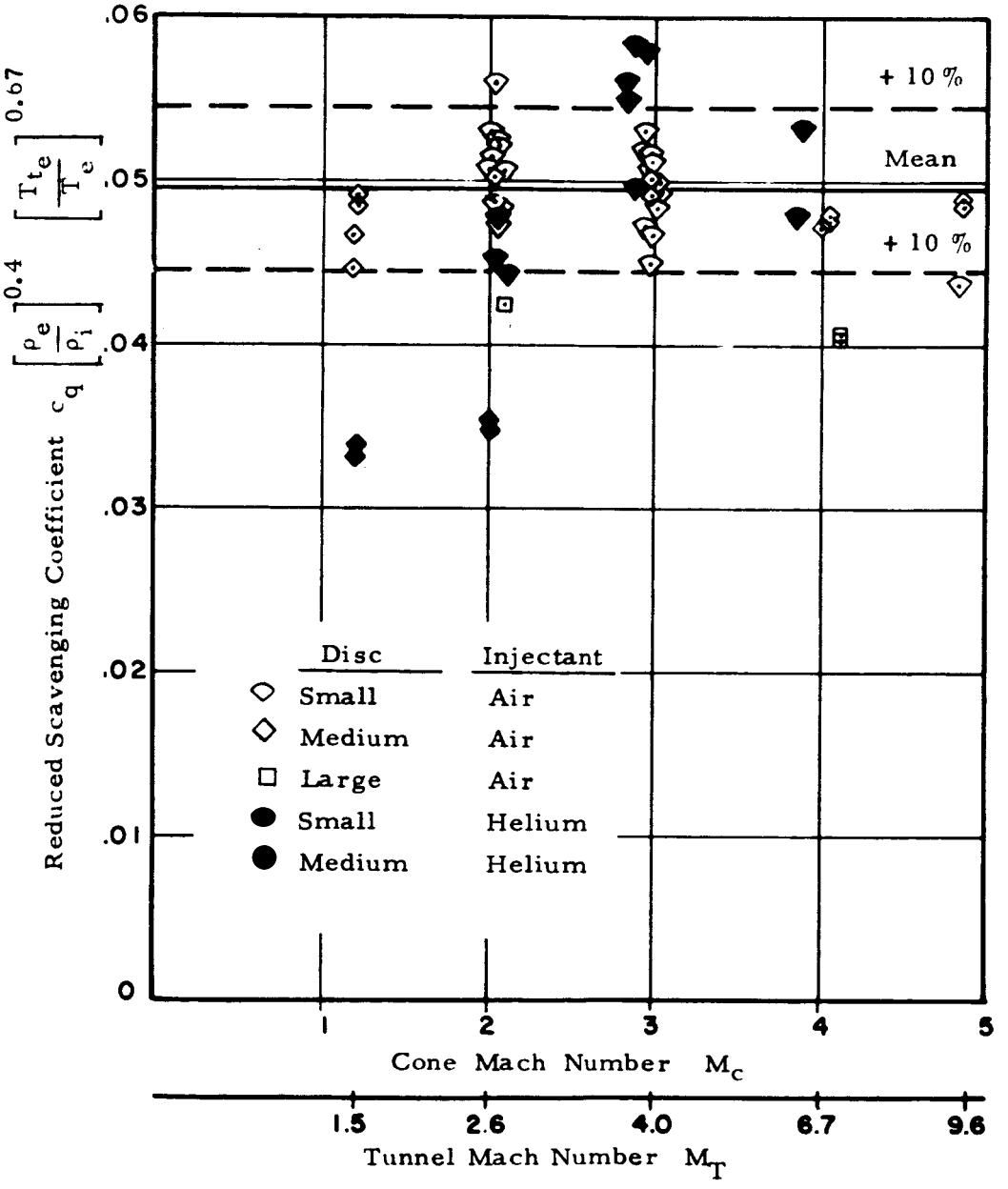

Figure 10. Summary plot of the correlation of all the data by the formula (12).

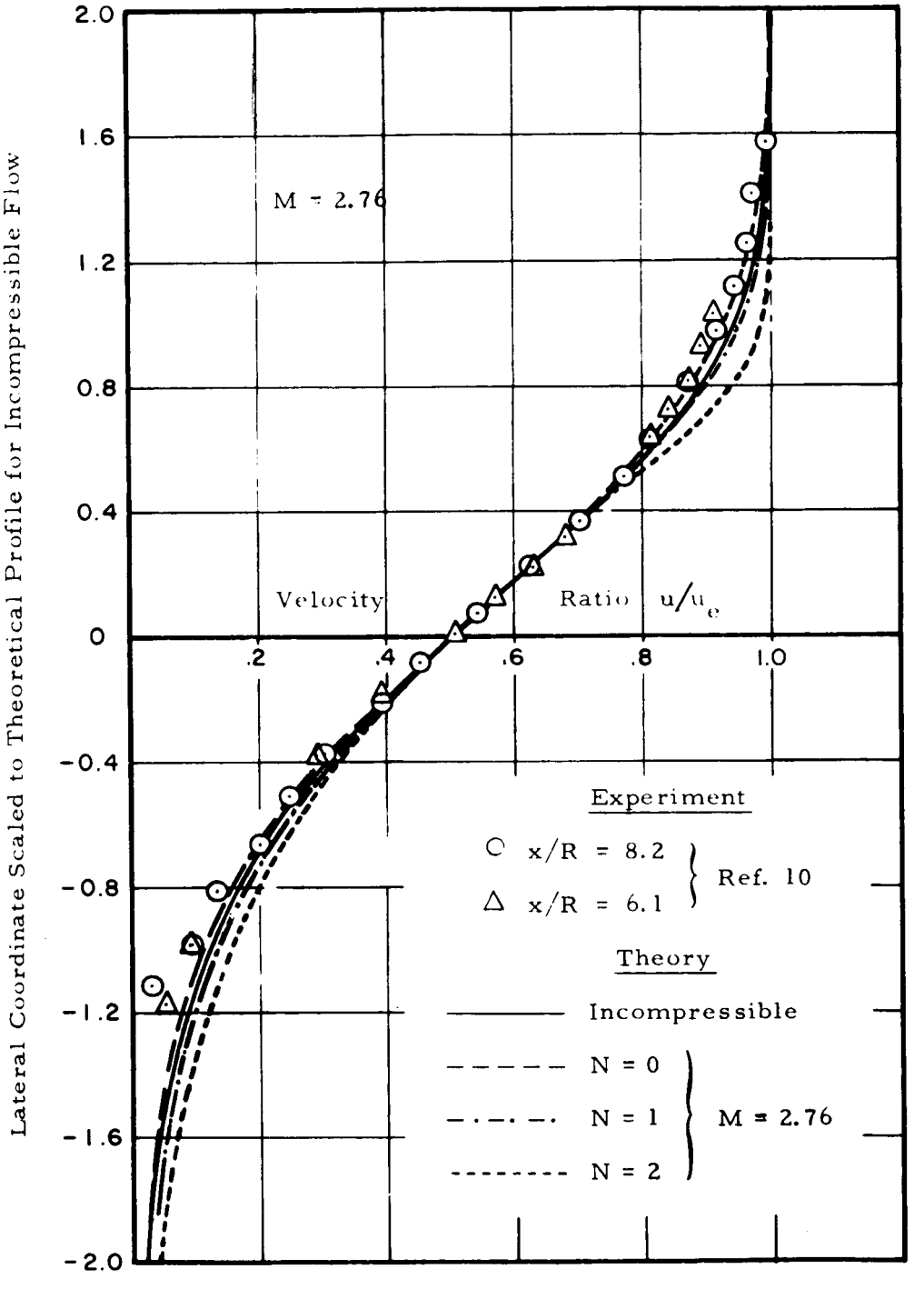

Figure 11. Comparison of profiles calculated with various values of N (Eq. 26) with measurements at M = 2.76.

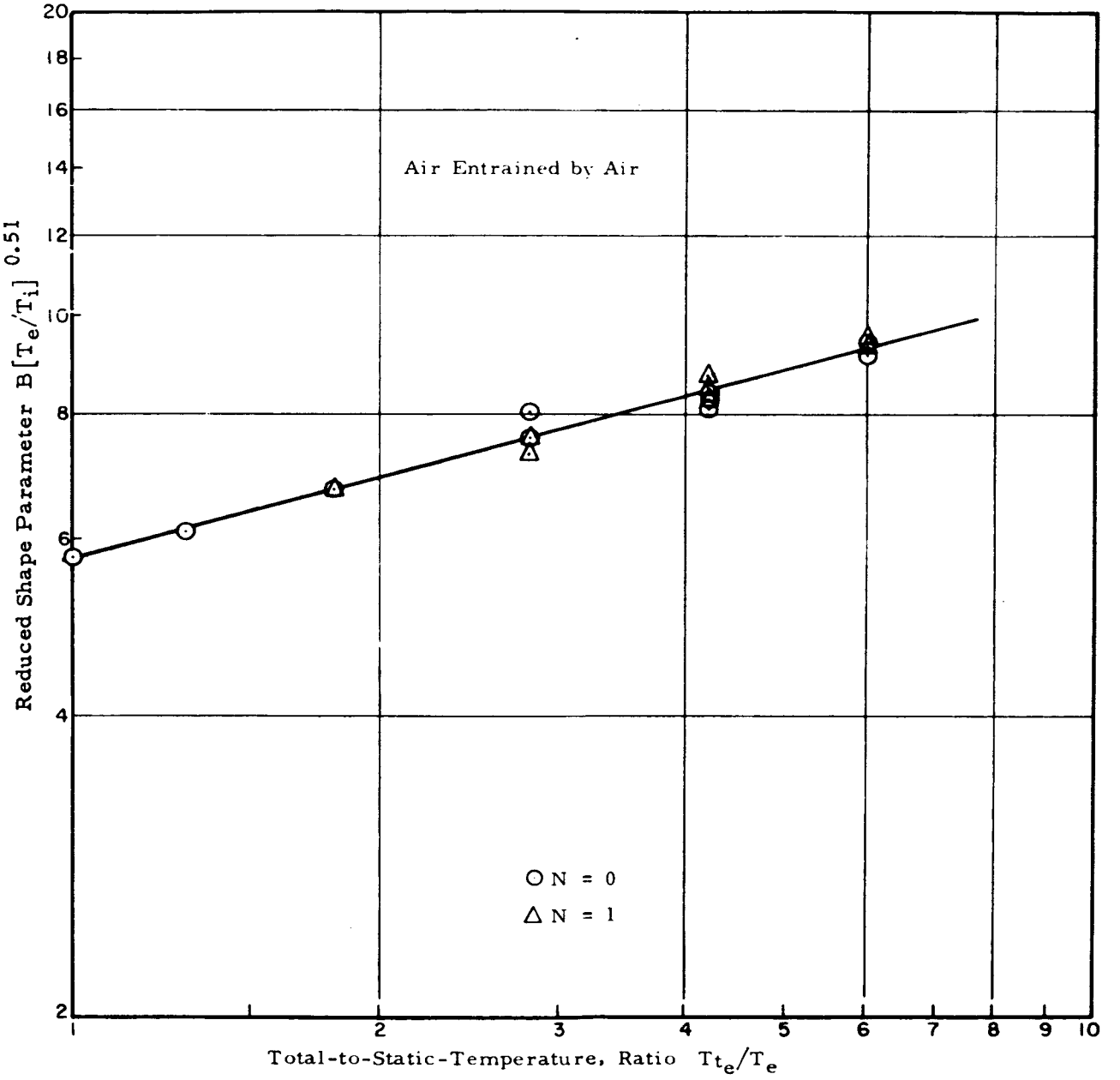

Figure 12. Reduced shape parameter $B(T_e/T_i)^{0.51}$ plotted against the total-to-static temperature ratio, T_{t_e}/T_e, of the external stream; air injection.

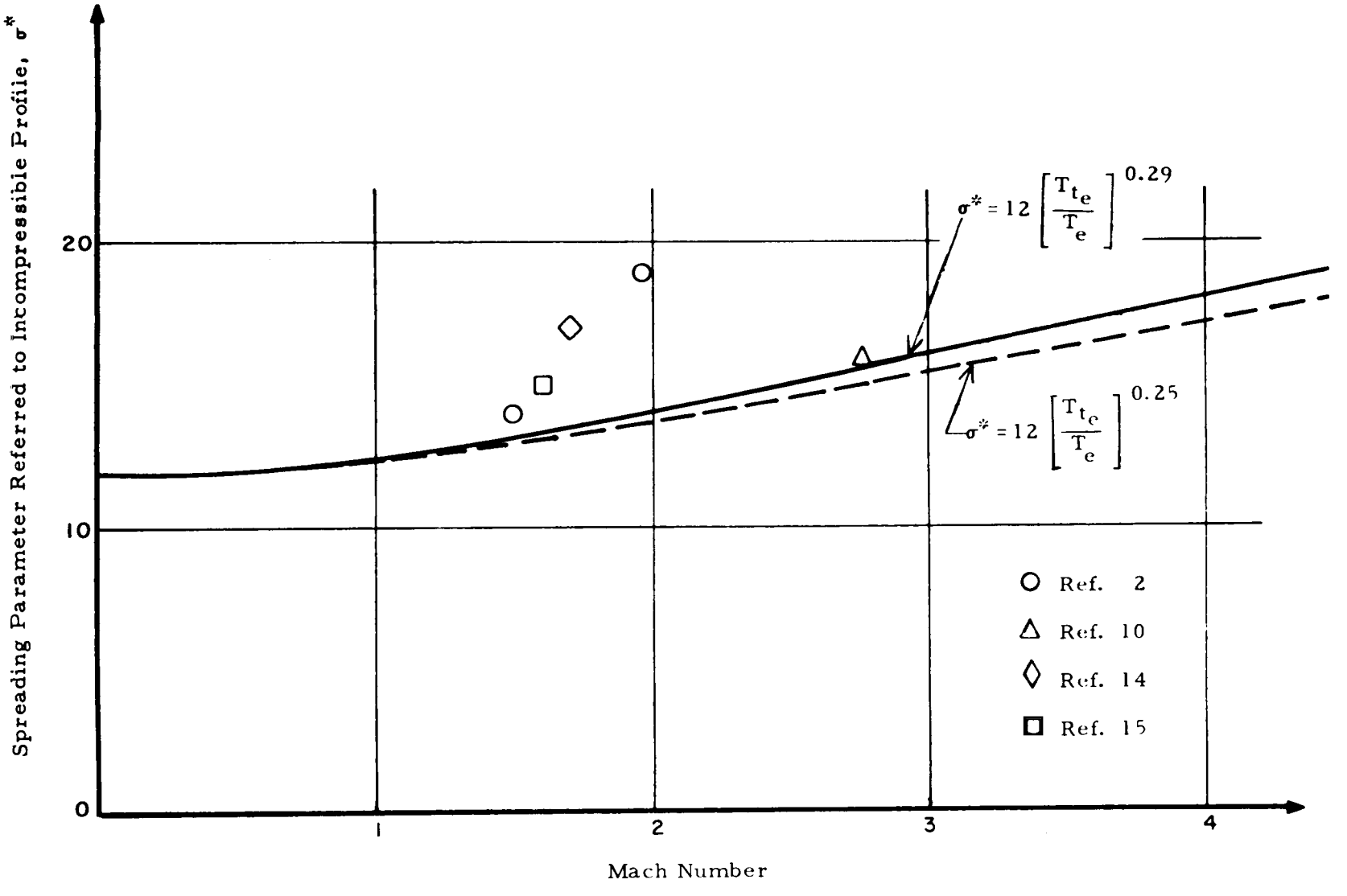

Figure 13. Spreading parameter σ^* plotted against Mach number for the isoenergetic flow of air into air; comparison of equation (57) with other measurements.

APPENDIX A

Symbols

b	width of mixing layer
b	shape parameter defined by equation (48)
c	mixing ratio by weight of foreign gas
c_p	specific heat at constant pressure
c_q	two-dimensional entrainment coefficient
c_q'	conical entrainment coefficient
f	reduced stream function, defined by equation (28)
G	mass flow per unit area
h	specific enthalpy
H	total enthalpy, $h + \frac{1}{2}u^2$
k	constant in the eddy-viscosity formula (24)
$\dot{m}$	entrained mass flow rate
m	molecular weight
M	Mach number
M_T	wind-tunnel Mach number
N	exponent of the density ratio in the viscosity law
p	pressure
T	temperature
T_t	total temperature
u	velocity component parallel to the mainstream in the mixing layer
v	velocity component perpendicular to the mainstream in the mixing layer
x	coordinate parallel to the mainstream
y	coordinate perpendicular to the mainstream

γ ratio of specific heats

δ width of the mixing layer expressed in terms of similarity variable, η

ϵ eddy viscosity

ϵ_0 constant in the evaluation of eddy viscosity

η similarity variable, $\sigma\frac{y}{x}$

ρ density

σ mixing-layer spreading parameter in two-dimensional flow

σ' mixing-layer spreading parameter in axisymmetric flow

σ^* mixing-layer spreading parameter referred to the theoretical profile for incompressible flow

ψ stream function

Subscripts

∞ freestream value

c cone-surface value

e at the outer edge of the mixing layer

i at the inside edge of the mixing layer

Superscript

* normalized quantity by reference to the outer edge of mixing layer

APPENDIX B

Transformation of the Equations of Motion for a Conical Mixing Layer to Two-Dimensional Form

Using the same assumptions as in the statement of the system of equations (13), the equations of motion for an axisymmetric turbulent mixing layer may be written

$$\frac{\partial}{\partial x}(\rho u y) + \frac{\partial}{\partial y}(\rho v y) = 0 \tag{B.1a}$$

$$\rho u \frac{\partial u}{\partial x} + \rho v \frac{\partial u}{\partial y} = \frac{1}{y} \frac{\partial}{\partial y}\left(\rho \epsilon y \frac{\partial u}{\partial y}\right) \tag{B.1b}$$

$$\rho u \frac{\partial c}{\partial x} + \rho v \frac{\partial c}{\partial y} = \frac{1}{y} \frac{\partial}{\partial y}\left(\rho \epsilon y \frac{\partial c}{\partial y}\right) \tag{B.1c}$$

$$\rho u \frac{\partial H}{\partial x} + \rho v \frac{\partial H}{\partial y} = \frac{1}{y} \frac{\partial}{\partial y}\left(\rho \epsilon y \frac{\partial H}{\partial y}\right) \tag{B.1d}$$

As in the two-dimensional case, the enthalpy, H, and mixing ratio, c, may be expressed as linear functions of the velocity, u. The momentum and continuity equation may be combined into a single ordinary differential equation, defining a self-similar flow, by introducing a similarity variable and stream function as before.

The similarity variable is written

$$\eta = \sigma' \frac{\bar{y}}{x} \tag{B.2}$$

where $\bar{y}$ is the transformed radial coordinate

$$\bar{y} = \int_{y_o}^{y} \frac{y}{y_o} \, dy \tag{B.3}$$

and y_o is the radial coordinate of the mean surface in the layer. The stream function is written

$$\psi = \frac{y_o x}{\sigma'} \frac{\rho_e u_e}{2} f(\eta) \tag{B.4}$$

and the continuity equation is satisfied by writing

$$\frac{\partial \psi}{\partial y} = \rho u y \qquad : \qquad \frac{\partial \psi}{\partial x} = - \rho v y \tag{B.5}$$

The velocity components in terms of the new variables are given by

$$\rho u = \frac{\rho_e u_e}{2} \frac{df}{d\eta} \tag{B.6}$$

$$\rho v = \frac{\rho_e u_e}{2\sigma} \frac{y_o}{y} \left[\eta \frac{df}{d\eta} - 2 f \right] \tag{B.7}$$

In particular, the entrainment coefficient

$$c_q' = \frac{(\rho v)_i}{\rho_e u_e} = - \frac{y_o}{y_i} \frac{f(-\infty)}{\sigma'} \tag{B.8}$$

where y_i is the radial coordinate of the inner edge of the mixing layer.

As in the two-dimensional case, it is necessary to know the behavior of the eddy-viscosity coefficient before the momentum equation can be written. For this purpose we postulate that the turbulent transport phenomena which define ϵ are essentially determined by the local flow conditions, and on this basis are not affected by the transverse curvature of the flow. Thus we write

$$\epsilon = k \left[\frac{\rho_e}{\rho} \right]^N b u_e \tag{B.9}$$

with b again the local thickness of the layer and postulate that the value of k is the same as in the two-dimensional flow.

The momentum equation transformed to an ordinary differential equation is then

$$f \frac{d}{d\eta} \left[\frac{\rho_e}{\rho} \frac{df}{d\eta} \right] + k \delta \sigma' \frac{d}{d\eta} \left[\left[\frac{\rho_e}{\rho} \right]^{N-1} \left[\frac{y}{y_o} \right]^2 \frac{d}{d\eta} \left[\frac{\rho_e}{\rho} \frac{df}{d\eta} \right] \right] = 0 \tag{B.10}$$

In order to obtain an equation of the form (35), it is necessary to make an approximation. If the thickness of the mixing layer is small

compared with the radial coordinate of the mean surface, the term $(y/y_o)^2$ varies only a small amount on each side of unity. We therefore equate it to unity and neglect its variation. An equation identical with (35) is then obtained if

$$\sigma' \approx \frac{1}{2k\delta} \tag{B.11}$$

A comparison of this expression with the corresponding formula (34) for the two-dimensional flow shows that

$$\sigma' \approx 2\sigma \tag{B.12}$$

or that the rate of spread of the conical layer is half that of the two-dimensional layer.

The flow in a mixing layer whose mean surface is a cone is thus similar to that in a two-dimensional layer, since it is governed by the same differential equation (35). Calculations or measurements obtained for either geometry may be applied to the other by use of the transformation developed here. In particular, the ratio of entrainment coefficients in the two flows is

$$\frac{c_q}{c_q'} \approx \frac{y_i}{y_o} \tag{B.13}$$

APPENDIX C

Correction of Mixing-Layer Growth Measurements Obtained in a Round Jet

The measurements on turbulent mixing layers reported by Maydew and Reed (Ref. 2) were obtained at the edge of a round jet exhausting into still air. In their discussion, these authors treat the data as if they had been obtained in a two-dimensional flow. This assumption is good if

(a) the mixing layers are thin compared with the diameter of the jet

(b) the mean surface of the mixing layer is cylindrical (i.e., does not increase in diameter)

Condition (a) is reasonably well satisfied near the exit of the nozzle from which the jet flows. Examination of the data shows, however, that a conical spread of the jet begins immediately from the nozzle exit so that condition (b) is not satisfied.

The effects of this conical spread on mixing layer growth may be described qualitatively as follows. Fluid entrained from the still-air region surrounding the jet is absorbed not only by a growth in the thickness of the mixing layer, but also by an increase in its lateral dimensions, or jet perimeter. Thus the rate of increase of the thickness is less than it would be if the flow were two-dimensional, or axisymmetric with a constant perimeter, if the entrainment rate remains fixed.

The transformation developed in Appendix B shows that the assumption of a fixed entrainment rate is a good one, since for these layers ($y_i/y_o \approx 1$) equation (B.13) states the entrainment rates of conical and two-dimensional layers are identical

$$c_q \approx c_q' \tag{C.1}$$

An approximate correction to the results published in Ref. 2 may be calculated by assuming that this result holds in the conically divergent flow from a round nozzle. In such a flow the equation of the mean surface of the mixing layer may be written

$$y_o = c_1 + c_2 x \tag{C.2}$$

and the total fluid entrained up to station x is, for a thin layer,

$$2\pi \rho_e u_e c_q \int y_o \, dx$$

$$= 2\pi \rho_e u_e x c_q \left(c_1 + \frac{1}{2} c_2 x\right) \tag{C.3}$$

The total quantity of entrained fluid carried along by the mixing layer at any station is proportional to the local thickness b' and the perimeter $2\pi y_o$. In terms of the shape-parameter B defined by equation (48) we may write

$$\dot{m} = \frac{2\pi}{B} \rho_e u_e b' (c_1 + c_2 x) \tag{C.4}$$

Equating this to (C.3) and solving for b' we obtain

$$b' = \frac{c_1 + \frac{1}{2} c_2 x}{c_1 + c_2 x} B c_q x \tag{C.5}$$

Now in two-dimensional flow, equation (53) shows that the mixing layer width b grows according to the equation

$$b = B c_q x \tag{C.6}$$

If we assume, then, that the value of B in the flow of the round jet is the same as in the two-dimensional flow, we can reduce the measured values of b' to equivalent two-dimensional thicknesses by computing

$$b = \frac{c_1 + c_2 x}{c_1 + \frac{1}{2} c_2 x} b' \tag{C.7}$$

Note that for a conical flow starting from a pointed nose this expression becomes

$$b = 2b' \tag{C.8}$$

which is exactly equivalent to the transformation of Appendix B, if the mixing layer is very thin.

The correction (C.7) has been applied point-by-point to the b' measurements of Ref. 2 and values of the spreading parameter σ^* have been obtained from plots of b against x.

APPENDIX D

Application of the Howarth-Dorodnitsyn Transformation to Mixing Layers in Compressible Flow

As noted in the review of mixing layer theory, use of the value $N = 2$ in the formula (26) for the eddy-viscosity coefficient allows the basic differential equation (35) to be transformed to the incompressible form (36).

The required transformation is

$$Y = \int \frac{\rho}{\rho_e} \, d\eta \tag{D.1}$$

where ρ_e is the density of the moving stream. With this transformation we obtain the equation

$$2f \frac{d^2 f}{dY^2} + \frac{d^3 f}{dY^3} = 0 \tag{D.2}$$

if the spreading parameter is chosen to be

$$\sigma = \frac{1}{4k\delta} \tag{D.3}$$

as before. The transformed boundary conditions are

$$f'(+\infty) = 2 \qquad f'(-\infty) = 0$$

and define the solution of (D.2) corresponding to a mixing layer in incompressible flow.

Since $f(-\infty)$ is thus unaffected by compressibility, any such effects on the entrainment coefficient

$$c_q = -\frac{f(-\infty)}{2\sigma} \tag{3}$$

must appear due to changes in σ. No information about this can be obtained from the transformation.

A possible method of proceeding with this theory is to borrow from the results of the corresponding theory for the fully developed round jet. Boynton (Ref. 16) has correlated jet spreading data in a form equivalent to writing

$$\sigma \propto \sqrt{T_{te} T_i} / T_e$$

Here the factor $\sqrt{T_i/T_e}$ was deduced from the transformation by applying a momentum conservation law. The remaining factor $\sqrt{T_{te}/T_e}$ was obtained as an approximate fit to data obtained at two Mach numbers.

REFERENCES

1. Tollmien, W. Berechnung der turbulenten Ausbreitungs-vorgänge. ZAMM Vol. 6, 1926, pp. 468-478 (Also NACA TM 1085, 1945).

2. Maydew, R. C. and Reed, J. F. Turbulent Mixing of Axisymmetric Compressible Jets (in the Half-Jet Region) with Quiescent Air. Research Report SC-4764(RR), Sandia Corporation, March 1963.

3. Ricou, F. P. and Spalding, D. B. Measurements of Entrainment by axisymmetrical Turbulent Jets-Jour, Fluid Mech. Vol. 11, Part I, August 1961. pp 21-32.

4. Chapman, D. R. The Laminar Mixing of a Compressible Fluid. NACA Report 948, 1950.

5. Prandtl, L. Bemerkungen zur Theorie der freien Turbulenz. ZAMM, Vol. 22, 1942.

6. Crane, L. J. The Laminar and Turbulent Mixing of Jets of Compressible Fluid. Jour. Fluid Mech. Vol. 3, Part I, October 1957.

7. Ferri, A., Libby, P. A., and Zakkay, V. Theoretical and Experimental Investigation of Supersonic Combustion. Report No. 713, Polytechnic Institute of Brooklyn, Department of Aerospace Engineering and Applied Mechanics, Sept,, 1962.

8. Ting L., and Libby P. Remarks on the Eddy Viscosity in Compressible Mixing Flows. J. A. S., Vol. 27, No. 10, October 1960

9. Görtler, H. Berechnung von Aufgaben der freien Turbulenz auf Grund eines neuen Näherungsansatzes. ZAMM Vol. 22, 1942, pp. 244-254.

10. Chrisman, C. C. Evaluation of the Free Jet Spreading Rate Parameter for Axisymetric Flow of Air at Mach Number three. M. S. thesis, Oklahoma State University, August 1962.

11. Rosler, R. S. Comment on "Turbulent Mixing of Compressible Free Jets". AIAA Journal, Vol. 1, No. 10, October 1963 pp. 2413-2414.

12. Liepman, H. W., and Laufer, J. Investigation on Free Turbulent Mixing. NACA TN 1257, 1947.

13. Reichardt, H. Gesetzmässigkeiten der freien Turbulenz. VD I - Forschungsheft 414, 1942, 2nd edition 1951.

14. Bershader, D. and Pai, S. L. On Turbulent Mixing in Two Dimensional Supersonic Flow. Journal of Applied Physics, Vol. 21, No. 6, 1950.

15. Gooderum, P. B., Wood, G. P., and Brevoort, M. J. Investigation with an Inter ferometer of the Turbulent Mixing of a Free Supersonic Jet. NACA TR 963, 1950.

16. Boynton, F. P. Self-Preservation in Fully Expanded Round Turbulent Jets. AIAA Journal, Vol. 1, No. 9, pp. 2176 - 2178.